

Iterative Learning Embedded Model Reference Adaptive Control for Perturbed Nonlinear MIMO Systems

Heng Zhang, Qilong Zhang, Song Liu, Yang Wang

Abstract—This paper presents a novel adaptive iterative learning control (ILC) framework for achieving high-performance trajectory tracking in uncertain nonlinear systems perturbed by external disturbances. The proposed scheme, referred to as IL-MRAC, combines two components inspired by indirect ILC and classical model reference adaptive control (MRAC), respectively. The key idea behind the proposed scheme is to first develop an input signal for a stabilized nominal model of the plant in ILC-loop, then inject the signal into the MRAC-Loop as the reference signal. This bypasses the unrealistic identical initialization condition required by conventional ILC methods and ingeniously transfers the problems brought by the initial errors, model uncertainties, and external disturbances to a powerful adaptive controller and handled in the time domain. Meanwhile, by including the well-trained inputs obtained in the iteration domain as reference signals, the adaptive controller gains the ability to directly track the desired trajectory. The convergence of the scheme is rigorously proven, and numerical examples and high-fidelity simulations demonstrate its effectiveness and superiority.

I. INTRODUCTION

Many industrial processes, such as manipulator tasks [1], air traffic management systems [2], and high-speed trains [3], involve repetitive tasks and are subject to external disturbances and model uncertainties. For such systems, the ultimate control goal is always to try to improve the transient behavior as well as maintain good robustness with respect to external disturbances and parameter uncertainties. Numerous methods have emerged that address these issues separately. For example, iterative learning control (ILC) take advantage of repetitive control task to achieve perfect tracking [4], [5] and adaptive control [6] and robust control [7] communities primarily focus on the issue of parameter uncertainty and unknown external disturbance. Next, we will provide a more detailed review of the ILC methodology and a classic adaptive approach to reveal the motivation behind this work.

ILC is essentially a feedforward control technology [8] that aims to improve the transient performance of the controlled system in repetitive tasks. However, its assumptions, such as identical initial conditions [9], the invariant of reference trajectories [10] and system parameters [11], may not be satisfied in practice due to output noise and uncertainties, which can degrade performance. To address this issue, many studies have been conducted to relax the requirement of strict repetitiveness in ILC. A common approach is to

This work was supported in part by the Yangfan Program of Shanghai, China, under Grant 21YF1429600. (*Corresponding author: Yang Wang*)

The authors are with the School of Information Science and Technology, ShanghaiTech University, Shanghai 201210, China {zhangheng1, zhangq11, liusong, wangyang4}@shanghaitech.edu.cn

aim for bounded iterative convergence performance using contraction mapping methods [12], assuming bounded uncertainties between iterations. Alternatively, some adaptive ILC schemes [13], [14] and rectifying mechanisms [15], [16] have been proposed to solve this problem in the time domain. While these methods do relax certain strict assumptions of ILC to tolerate more uncertainty, they sacrifice either the performance or simplicity of the algorithm.

On the other hand, adaptive methods are particularly effective in dealing with non-repetitive uncertainties. Among various existing solutions, one of the most well-known and mature approaches is the model reference adaptive control (MRAC) strategy [17], [18]. In MRAC [6], the desired performance is specified by a user-defined reference model, while the controller's mission is to drive the plant's output to follow the output of the reference model. Designing a reference model that generates the desired response for any given trajectory is challenging even for control engineers. Moreover, the reference model is essentially a command-shaping filter that achieves a desired command following [19]. This limitation means that the MRAC scheme can only track the output of the reference model, rather than directly tracking the reference signal itself.

As discussed above, a straightforward attempt is to combine the ILC and MRAC [20]–[22] while retaining their respective advantages. Although some effort has been made toward this purpose, the majority of existing techniques are under the direct ILC framework. This leads to online training, which is infeasible in most practical applications. This paper presents a new IL-MRAC framework that combines indirect ILC and classical MRAC in a novel way to solve the aforementioned difficulties to a large degree. To the best of the authors' knowledge, this is the first indirect ILC scheme that guarantees stability in the presence of large perturbations, preserves the high performance provided by the ILC components, and endows the MRAC component with the ability to directly track the desired signal.

The combination of ILC and MRAC is not a trivial task. One of the key techniques we used for integration is to replace the reference model in the MRAC algorithm with the nominal model of the controlled process governed by a stabilizing controller. By doing so, the scheme essentially removes the need to design a reference model. The IL-MRAC framework achieves high-performance tracking by iteratively modifying the input signals of the reference model, and then using the well-trained input signals as reference signals for the MRAC-loop. This approach offers several advantages. First, the MRAC-loop accounts for the effect

of model uncertainties, external disturbances, and unknown initial states, eliminating the need to consider them in the iteration domain. Second, it requires less effort and time for MRAC to track its nominal model compared to tracking a delicately designed reference model, as done in classic MRAC. Finally, the iteration can be carried out in an offline and numerical manner, reducing the training cost that may be a significant concern in practical applications. In addition, for systems that satisfy the principle of superposition, the computational burden can be further reduced by combining pre-trained input signals to obtain optimal reference signals. Our theoretical analysis provides clear conditions that each component (i.e. ILC-loop and MRAC-loop) needs to satisfy to ensure the stability and robustness of the overall system. As a result, each component can potentially be replaced by a more advanced version, if available.

Notation: \mathbb{R}^n and $\mathbb{R}^{n \times m}$ denote the sets of n dimensional real vectors and $n \times m$ real matrices respectively; \mathbb{R}^+ and \mathbb{Z}^+ respectively denote the positive real constant and positive integer, $\|A\|$ denotes any matrix (or vector) norm of a matrix (or vector) A ; $\|A\|_2$ denotes 2-norm of a matrix (or vector) A ; the identity and zero matrices (vectors) of compatible dimensions are denoted by \mathbf{I} and $\mathbf{0}$, respectively; \mathbf{b}^\dagger represents the pseudo inverse of matrix \mathbf{b} ; \mathcal{I}_n^m represents a set of selecting m elements from n elements, $m \leq n$. Other notations will be introduced as needed.

II. SYSTEM DESCRIPTION AND PROBLEM FORMULATION

Consider a class of high-order MIMO nonlinear dynamical systems described by

$$\begin{aligned}\dot{\mathbf{x}}_i(t) &= \mathbf{x}_{i+1}(t), \quad i = 1, \dots, p-1 \\ \dot{\mathbf{x}}_p(t) &= \mathbf{h}(\mathbf{x}, \mathbf{p}, t) + \mathbf{b}(\mathbf{z}, \mathbf{p}, t)[\mathbf{u} + \mathbf{f}(\mathbf{x}, \mathbf{p}, t, \omega)]\end{aligned}\quad (1)$$

where $\mathbf{x}_i(t) \in \mathbb{R}^{l \times 1}$, $i = 1, \dots, p$, and $t \in [0, T_f]$ with $T_f \in \mathbb{R}^+$, $\mathbf{x} \triangleq [\mathbf{x}_1^\top, \mathbf{x}_2^\top, \dots, \mathbf{x}_p^\top]^\top \in \mathbb{X} \subseteq \mathbb{R}^{n \times 1}$ is the measurable state vector of the system by using the notation $n \triangleq pl$. $\mathbf{u} \in \mathbb{R}^{m \times 1}$ is the control input vector of the system. $\mathbf{z} \in \mathbb{Z} \subseteq \mathbb{R}^{q \times 1}$ where \mathbb{Z} is a subset of the state space \mathbb{X} with dimension $q \leq n$. $\mathbf{p} \in \mathbb{P}$ is an unknown system parameter vector. \mathbb{P} is the set of admissible system parameters. $\mathbf{h}(\mathbf{x}, \mathbf{p}, t)$ represents the structured uncertainties and $\mathbf{f}(\mathbf{x}, \mathbf{p}, t, \omega)$ represents unstructured uncertainties. $\omega \in \mathbb{R}$ represents any aperiodic factor such as aperiodic exogenous disturbances or system noise. $\mathbf{b}(\mathbf{z}, \mathbf{p}, t) \in \mathbb{R}^{l \times m}$ is the input distribution matrix. In practical applications, the form of system (1) can be widely seen in the industry, for example, in the multi-joint manipulator system [1], \mathbf{x}_1 and \mathbf{x}_2 represent the joint angle and velocity, respectively. Roughly speaking, our control objective is to find a proper input $\mathbf{u}(t)$ for system (1) to track a given trajectory $\mathbf{x}_d(t)$. To proceed, we first make the following assumptions:

Assumption 1: For all $t \in [0, T_f]$, $\mathbf{z} \in \mathbb{Z}$, $\mathbf{p} \in \mathbb{P}$, the input matrix $\mathbf{b}(\mathbf{z}, \mathbf{p}, t)$ is a column full rank matrix with $l = m$ and can be expressed as $\mathbf{b}(\mathbf{z}, \mathbf{p}, t) = \mathbf{b}_0(\mathbf{z}, \mathbf{p}, t)\boldsymbol{\lambda}$ where $\mathbf{b}_0(\mathbf{z}, \mathbf{p}, t) \in \mathbb{R}^{l \times m}$ is a known nominal matrix, $\boldsymbol{\lambda} \triangleq \text{diag}(\lambda_1, \dots, \lambda_m) \in \mathbb{R}^{m \times m}$ is a diagonal matrix to represent the uncertainty of input matrix \mathbf{b} , and $\text{sign}(\boldsymbol{\lambda}) \triangleq$

$\text{diag}(\text{sign}(\lambda_1), \dots, \text{sign}(\lambda_m)) \in \mathbb{R}^{m \times m}$ is known. Without loss of generality, $\text{sign}(\boldsymbol{\lambda}) = \mathbf{I}$. \triangleleft

Assumption 2: The unknown function vector $\mathbf{h}(\mathbf{x}, \mathbf{p}, t)$ and $\mathbf{f}(\mathbf{x}, \mathbf{p}, t, \omega)$ can be expressed as

$$\begin{aligned}\mathbf{h}(\mathbf{x}, \mathbf{p}, t) &= \mathbf{a}\mathbf{x} + \boldsymbol{\theta}_1^\top(\mathbf{p})\phi_1(\mathbf{x}, t) \\ \mathbf{f}(\mathbf{x}, \mathbf{p}, t, \omega) &= \boldsymbol{\theta}_2^\top(\mathbf{p})\phi_2(\mathbf{x}, t) + \mathbf{d}(\omega, t)\end{aligned}$$

where $\mathbf{a} \in \mathbb{R}^{l \times n}$, $\boldsymbol{\theta}_1 \in \mathbb{R}^{s_1 \times l}$ and $\boldsymbol{\theta}_2 \in \mathbb{R}^{s_2 \times m}$ are unknown constant matrices, $\phi_1 \in \mathbb{R}^{s_1 \times 1}$ and $\phi_2 \in \mathbb{R}^{s_2 \times 1}$ are vectors of known and bounded basis functions, $\mathbf{d}(\omega, t) \in \mathbb{R}^{m \times 1}$ is the bounded non-parametric external disturbances. \triangleleft

Based on above assumptions, system (1) can be rewritten as:

$$\dot{\mathbf{x}} = A\mathbf{x} + B\Lambda[\mathbf{u} + \Theta_d^\top\Phi(\mathbf{x}) + \mathbf{d}(\omega, t)] \quad (2)$$

with $\Lambda = \boldsymbol{\lambda} \in \mathbb{R}^{m \times m}$, $\Theta_d \in \mathbb{R}^{s \times m}$, $\Phi(\mathbf{x}) \in \mathbb{R}^{s \times 1}$ and

$$A = \begin{bmatrix} \mathbf{0} & | & \mathbf{I} \\ \mathbf{a} & \end{bmatrix} \in \mathbb{R}^{n \times n} \quad B = \begin{bmatrix} \mathbf{0} \\ \mathbf{b}_0 \end{bmatrix} \in \mathbb{R}^{n \times m}$$

where $\Theta_d^\top\Phi(\mathbf{x}) \triangleq \mathbf{b}^\dagger\boldsymbol{\theta}_1^\top(\mathbf{p}, t)\phi_1(\mathbf{x}, t) + \boldsymbol{\theta}_2^\top(\mathbf{p}, t)\phi_2(\mathbf{x}, t)$ is the rearranged combination of parametric representations of uncertainties.

Assumption 3: For system (2), the pair $(A, B\Lambda)$ and the pair (A_0, B_0) are controllable, where A_0 and B_0 are the nominal parts of A and $B\Lambda$, respectively. \triangleleft

Property 1: For system (2), there always exists a trivial full-state feedback controller to render its nominal part into the following form

$$\dot{\mathbf{x}}_m = A_m\mathbf{x}_m + B_m\mathbf{r} \quad (3)$$

where $\mathbf{x}_m \in \mathbb{R}^n$, $A_m \in \mathbb{R}^{n \times n}$ is known and Hurwitz, $B_m = B \in \mathbb{R}^{n \times m}$ is a known and full column matrix, and $\mathbf{r}(t) \in \mathbb{R}^m$ is a piece-wise continuous and bounded command vector. Furthermore, by introducing the iteration variable k as the state argument, the identical initialization condition of the dynamics of (3) holds naturally for all iterations, i.e. $\mathbf{x}_m(k, 0) = \mathbf{r}(0)$, for all $k \in \mathbb{Z}^+$. \triangleleft

Assumption 4: For a given differentiable and bounded trajectory $\mathbf{x}_d(t)$, there exists a unique bounded $\mathbf{r}_d(t)$, $\forall t \in [0, T_f]$, such that $\dot{\mathbf{x}}_d = A_m\mathbf{x}_d + B_m\mathbf{r}_d$, $\mathbf{x}_d(0) = \mathbf{x}_m(0)$. \triangleleft

Consider a state feedback control law

$$\mathbf{u}^*(t) = K_{x,d}\mathbf{x}(t) + K_{r,d}\mathbf{r}(t) - \Theta_d^\top\Phi(\mathbf{x}) \quad (4)$$

where $K_{x,d} \in \mathbb{R}^{m \times n}$ and $K_{r,d} \in \mathbb{R}^{m \times m}$ are gain matrices to be specified. Substituting (4) in (2) yields

$$\dot{\mathbf{x}}(t) = (A + B\Lambda K_{x,d})\mathbf{x}(t) + B\Lambda K_{r,d}\mathbf{r}(t) + B\Lambda\mathbf{d}(t) \quad (5)$$

To match the closed-loop system (5) to the nominal model (3), the following matching condition is needed:

Assumption 5: [23] There exist time-invariant matrices gains $K_{x,d}$ and $K_{r,d}$ such that

$$A + B\Lambda K_{x,d} = A_m, \quad B\Lambda K_{r,d} = B_m. \quad \triangleleft$$

Remark 1: Note that, if A_m and B_m have the same structures as those of A and $B\Lambda$, respectively, or if $B\Lambda$ is a square and invertible matrix, then the existence of $K_{x,d}$ and $K_{r,d}$ are ensured. \triangleleft

Now, the control objective becomes to find a proper $\mathbf{u}(t)$ to drive states of the nonlinear MIMO system (2) to track the desired trajectory $\mathbf{x}_d(t)$, while reducing the negative effects

of model uncertainties, external disturbances, and unknown system initial states. To this end, the IL-MRAC scheme with the structure shown in Fig. 1 is adopted. In addition, a crucial signal $\mathbf{r}(k, t)$ that updates with iteration will be utilized as a bridge between ILC and MRAC. Before proceeding to the control scheme, the following lemma regarding the Hurwitz matrix is introduced.

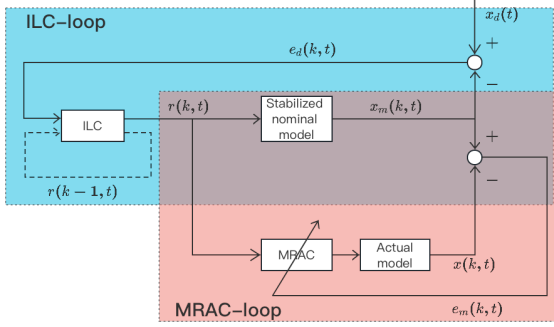


Fig. 1. Schematic diagram of the IL-MRAC scheme.

Lemma 2.1: For any Hurwitz matrix A_m and a symmetric semi-positive definite matrix N , the eigenvalues of $A_m N$ are less than or equal to 0. \triangleleft

Proof: Suppose λ is an eigenvalue of $A_m N$ with eigenvector $\mathbf{x} \neq 0$, i.e. $A_m N \mathbf{x} = \lambda \mathbf{x}$. Then we have $N A_m N \mathbf{x} = \lambda N \mathbf{x}$, and $\mathbf{x}^\top N A_m N \mathbf{x} = \lambda \mathbf{x}^\top N \mathbf{x}$. The following proof will be divided into two folds: First, while $N \mathbf{x} \neq 0$, then for all $\mathbf{x} \neq 0$, we have $\mathbf{x}^\top N \mathbf{x} \neq 0$, more specifically, $\mathbf{x}^\top N \mathbf{x} > 0$ due to the non-negativity of matrix N . On the other hand, it is not hard to check that $N A_m N$ is negative definite since the following inequality holds for all $\mathbf{x} \neq 0$:

$$\mathbf{x}^\top N A_m N \mathbf{x} = (N \mathbf{x})^\top A_m (N \mathbf{x}) = \mathbf{z}^\top A_m \mathbf{z} < 0$$

where $\mathbf{z} = N \mathbf{x}$ represents the eigenvector of A_m . Hence, $\lambda = \mathbf{x}^\top N A_m N \mathbf{x} < 0$ in this case. Second, while $N \mathbf{x} = 0$ with eigenvector $\mathbf{x} \neq 0$, we have $A_m N \mathbf{x} = \lambda \mathbf{x} = 0$, that's to say, $\lambda = 0$. Thus, we have $\lambda \leq 0$ for all cases. \square

III. IL-MRAC SCHEME DESIGN

In this section, the proposed IL-MRAC scheme is introduced in detail. As elaborated in Fig. 1, the ILC-loop will be updated first to enable the reference model to achieve perfect tracking of the desired signal, then followed by the control of the MRAC-loop to ensure that the actual system can track the desired trajectory. Consider an ILC designed as

$$\mathbf{r}(k+1, t) = \mathbf{r}(k, t) + \frac{B_m^\top}{\|B_m B_m^\top\|} K \mathbf{e}_d(k+1, t) \quad (6)$$

where $\mathbf{r}(k, t) \in \mathbb{R}^m$ denotes the output of ILC controller at k -th iteration and time instant t . $\mathbf{e}_d(k, t) = [\mathbf{e}_{d,1}(k, t), \mathbf{e}_{d,2}(k, t), \dots, \mathbf{e}_{d,n}(k, t)] \triangleq \mathbf{x}_d(t) - \mathbf{x}_m(k, t)$ represents the tracking error of the nominal model. $K \in \mathbb{R}^{n \times n}$ is a diagonal positive constant control gain matrix chosen to be cI with $c > 0$, for simplicity. $\mathbf{r}(k, t)$ is updated as the iteration increases until $\|\mathbf{e}_d(t)\| \leq \epsilon$ with a prescribed accuracy ϵ for all $t \in [0, T_f]$. For convenience in the following writing, we denote the trained $\mathbf{r}(k, t)$ as the $\mathbf{r}(t)$.

Then, the nominal model (3) and the actual plant (2) are connected as MRAC-loop, as shown in Fig. 1. Taking $\mathbf{r}(t)$ as the reference signal, we propose an adaptive controller as

$$\mathbf{u}(t) = K_x(t) \mathbf{x}(t) + K_r(t) \mathbf{r}(t) - \Theta^\top(t) \Phi(\mathbf{x}) \quad (7)$$

$$\dot{K}_x^\top = \Gamma_x \mathbf{x} \mathbf{e}_m^\top P B \text{sign}(\Lambda), \dot{K}_r^\top = \Gamma_r \mathbf{r} \mathbf{e}_m^\top P B \text{sign}(\Lambda) \quad (8)$$

$$\dot{\Theta} = -\Gamma_\Theta \Phi \mathbf{e}_m^\top P B \text{sign}(\Lambda) \quad (9)$$

where $K_x(t) \in \mathbb{R}^{m \times n}$, $K_r(t) \in \mathbb{R}^{m \times m}$, and $\Theta(t) \in \mathbb{R}^{s \times m}$ are estimates of $K_{x,d}$, $K_{r,d}$, and Θ_d defined in (4), respectively. $\Gamma_x, \Gamma_r, \Gamma_\Theta$ are positive-definite gain matrices of compatible dimensions. $P = P^\top \in \mathbb{R}^{n \times n}$ is a positive-definite matrix satisfying the Lyapunov equation

$$P A_m + A_m^\top P = -Q \quad (10)$$

for a given positive-definite $Q \in \mathbb{R}^{n \times n}$ with $\lambda_{\min}(Q) > 1$. In virtue of Property 1 and Assumption 5, the dynamic of the tracking error $\mathbf{e}_m(t) \triangleq \mathbf{x}_m(t) - \mathbf{x}(t)$ is given by

$$\dot{\mathbf{e}}_m = A_m \mathbf{e}_m - B \Lambda \tilde{K}_x \mathbf{x} - B \Lambda \tilde{K}_r \mathbf{r} + B \Lambda \tilde{\Theta}^\top \Phi - B \Lambda \mathbf{d} \quad (11)$$

where $\tilde{K}_x(t) \triangleq K_{x,d}(t) - K_x$, $\tilde{K}_r(t) \triangleq K_{r,d}(t) - K_r$, and $\tilde{\Theta} \triangleq \Theta_d - \Theta$ are estimation errors. Define the tracking error $\mathbf{e}(t) = [\mathbf{e}_1(t), \mathbf{e}_2(t), \dots, \mathbf{e}_n(t)] \triangleq \mathbf{x}_d(t) - \mathbf{x}(t)$ and $\rho^* \triangleq \text{rank}(B_m)$. We now state the main results of this article.

Theorem 3.1: Consider the nonlinear MIMO system (1) satisfying Assumptions 1–5. For all $t \in [0, T_f]$, the proposed IL-MRAC scheme given in (6)–(10) guarantees that
(T1) $\mathbf{e}_d(k, t)$ is bounded and $\lim_{k \rightarrow \infty} \|\mathbf{e}_{d,i}(k, t)\| = 0$, for all $i \in \mathcal{I}_n^{\rho^*}$, $k \geq 1$.
(T2) $\mathbf{e}_m(t)$ is bounded and $\lim_{t \rightarrow \infty} \|\mathbf{e}_m(t)\| = \gamma_1(\mathbf{d})$.
(T3) $\mathbf{e}(t)$ is bounded and $\lim_{t \rightarrow \infty} \|\mathbf{e}_i(t)\| = \gamma_2(\mathbf{d})$, $i \in \mathcal{I}_n^{\rho^*}$.
(T4) All the internal signals $\mathbf{r}(k, t)$, $\mathbf{x}_m(k, t)$, $\mathbf{x}(t)$ are bounded for all $k \geq 1$.

where $\gamma_1(\cdot)$ and $\gamma_2(\cdot)$ are some class- \mathcal{K} functions.

Proof: The proof mainly contains three steps. First, we show that, in ILC-loop, there is a composite energy function (CEF) bounded over $[0, T_f]$ and monotonically decreasing as $k \rightarrow \infty$, which leads to the statement in (T1). Second, the proof of MRAC-loop is given to support (T2). Subsequently, the conclusions in (T3) and (T4) can be easily obtained.

(T1): Given Assumption 3–4, the dynamic of the tracking error of $\mathbf{e}_d(k, t)$ follows:

$$\dot{\mathbf{e}}_d(k, t) = \dot{\mathbf{x}}_d(t) - \dot{\mathbf{x}}_m(k, t) = A_m \mathbf{e}_d(k, t) - B_m \tilde{\mathbf{r}}(k, t) \quad (12)$$

where $\tilde{\mathbf{r}}(k, t) \triangleq \mathbf{r}(k, t) - \mathbf{r}_d(t)$. Defining pseudo-inverse $B_m^\dagger \triangleq (B_m^\top B_m)^{-1} B_m^\top$, it holds

$$\tilde{\mathbf{r}}(k, t) = (B_m^\top B_m)^{-1} B_m^\top [-\dot{\mathbf{e}}_d(k, t) + A_m \mathbf{e}_d(k, t)] \quad (13)$$

The CEF is designed as

$$E_d(k, t) = \int_0^t \tilde{\mathbf{r}}^\top(k, \tau) \tilde{\mathbf{r}}(k, \tau) d\tau \quad (14)$$

Then, by virtue of (6), we have $\Delta E_d(k) \triangleq E_d(k) - E_d(k-1)$ admits the form of

$$\begin{aligned} \Delta E_d(k) &= \int_0^t \tilde{\mathbf{r}}^\top(k) \tilde{\mathbf{r}}(k) - \tilde{\mathbf{r}}^\top(k-1) \tilde{\mathbf{r}}(k-1) d\tau \\ &= \int_0^t - \left[\frac{B_m^\top K \mathbf{e}_d(k)}{\|B_m B_m^\top\|} - 2 \tilde{\mathbf{r}}(k) \right]^\top \frac{B_m^\top K \mathbf{e}_d(k)}{\|B_m B_m^\top\|} d\tau \end{aligned} \quad (15)$$

where we have made use of the fact that $\tilde{\mathbf{r}}^\top(k)\tilde{\mathbf{r}}(k-1)$ is a scalar, and take the advantages of (6). Time variable t is omitted without affecting readability.

In view of (13), $\Delta E_d(k, t)$ can be further simplified to

$$\begin{aligned}\Delta E_d(k, t) &= \int_0^t \left[\frac{B_m^\top \mathbf{e}_d(k)}{\|B_m B_m^\top\|} K + 2(B_m^\top B_m)^{-1} B_m^\top \dot{\mathbf{e}}_d(k) \right. \\ &\quad \left. - 2(B_m^\top B_m)^{-1} B_m^\top A_m \mathbf{e}_d(k) \right]^\top \frac{B_m^\top}{\|B_m B_m^\top\|} K \mathbf{e}_d(k) d\tau \quad (16)\end{aligned}$$

Then the monotonic decrease of $E_d(k, t)$ is conducted by showing the negativity or non-positivity of each term in (16).

For the first component, it is obvious that

$$-\int_0^t \left[\frac{B_m^\top}{\|B_m B_m^\top\|} K \mathbf{e}_d(k) \right]^\top \cdot \frac{B_m^\top}{\|B_m B_m^\top\|} K \mathbf{e}_d(k) d\tau \leq 0 \quad (17)$$

Then, by adopting the method of integration by parts, the second part of (16) is treated as follows:

$$\begin{aligned}-2 \int_0^t [(B_m^\top B_m)^{-1} B_m^\top \dot{\mathbf{e}}_d(k)]^\top \frac{B_m^\top}{\|B_m B_m^\top\|} K \mathbf{e}_d(k) d\tau \\ = -2 \int_0^t \dot{\mathbf{e}}_d^\top(k) M \mathbf{e}_d(k) d\tau = -\mathbf{e}_d^\top(k, t) M(t) \mathbf{e}_d(k, t) \quad (18)\end{aligned}$$

whose sign now depends on the symmetric matrix $M \triangleq \frac{N}{\|B_m B_m^\top\|} K$ with $N \triangleq B_m (B_m^\top B_m)^{-1} B_m^\top$. We briefly prove that the matrices M and N are semi-positive definite.

It's trivial to see that $B_m^\top B_m \in \mathbb{R}^{m \times m}$ is a symmetric semi-positive definite matrix as $\mathbf{x}^\top B_m^\top B_m \mathbf{x} = (B_m \mathbf{x})^\top B_m \mathbf{x} \geq 0$, for all $\mathbf{x} \in \mathbb{R}^n$. Thus, together with the fact that B_m is full column rank, the inverse of $B_m^\top B_m$ remains symmetric and semi-positive definite, such that the $(B_m^\top B_m)^{-1} = LL^\top$ holds by applying Cholesky decomposition, where L is a positive definite matrix. Therefore, $N = (B_m L)(B_m L)^\top$ is a symmetric semi-positive definite matrix due to the fact $(B_m L)^\top$ is not full column rank, and M is also semi-positive definite by its definition.

Finally, according to Property 1 and Lemma 2.1, for all $\mathbf{e}_d(k, t) \in \mathbb{R}^n$, the third part of (16) is analyzed as follows:

$$\begin{aligned}2 \int_0^t [(B_m^\top B_m)^{-1} B_m^\top A_m \mathbf{e}_d(k)]^\top \cdot \frac{B_m^\top}{\|B_m B_m^\top\|} K \mathbf{e}_d(k) d\tau \\ = 2 \int_0^t \mathbf{e}_d^\top(k) \frac{A_m^\top N}{\|B_m B_m^\top\|} K \mathbf{e}_d(k) d\tau \leq 0 \quad (19)\end{aligned}$$

In view of (17), (18) and (19), the difference of $E_d(k, t)$ in (16) can be further reduced as follows

$$\Delta E_d \leq -\mathbf{e}_d^\top(k) M \mathbf{e}_d(k) - \int_0^t \left\| \frac{B_m^\top}{\|B_m B_m^\top\|} K \mathbf{e}_d(k) \right\|_2^2 d\tau \leq 0 \quad (20)$$

From (20), it can be immediately obtained that

$$\begin{aligned}E_d(k, t) &= E_d(0, t) + \sum_{j=1}^k \Delta E_d(j, t) \\ &\leq E_d(0, t) - \sum_{j=1}^k [\mathbf{e}_d^\top(k, t) M \mathbf{e}_d(k, t) + \int_0^t \left\| \frac{B_m^\top}{\|B_m B_m^\top\|} K \mathbf{e}_d(k) \right\|_2^2 d\tau]\end{aligned}$$

According to the definition of CEF (14) and Property 1, it is easy to see that $E_d(0, t)$ is bounded. In view of (20), we can obtain that the $\tilde{\mathbf{r}}(k, t)$ is bounded as $k \rightarrow \infty$, for all $t \in [0, T_f]$. By using (6) and the fact that $\mathbf{r}_d(t)$ is a bounded signal, it follows that as $k \rightarrow \infty$, $\mathbf{r}(k, t)$ is also

bounded. This, in turn, implies that the state $\mathbf{x}_m(t)$ of (3) is also bounded. In addition, in view of the fact that the desired trajectory $\mathbf{x}_d(t)$ is bounded, we can conclude that $\mathbf{e}_d(k, t)$ is also bounded. Additionally, considering the structure of N , it includes a positive definite block of rank ρ^* , which results in the error of certain states in (20) converging to zero as the iterations progress, i.e. $\lim_{k \rightarrow \infty} \|\mathbf{e}_{d,i}(k, t)\| = 0$, $\forall i \in \mathcal{I}_n^{\rho^*}$.

(T2): Consider another CEF for MRAC-loop as follows:

$$\begin{aligned}V(\mathbf{e}_m, \tilde{K}_x, \tilde{K}_r, \tilde{\Theta}) &= \mathbf{e}_m^\top P \mathbf{e}_m + \text{trace}(|\Lambda| \tilde{K}_x \Gamma_x^{-1} \tilde{K}_x^\top) \\ &\quad + \text{trace}(|\Lambda| \tilde{K}_r \Gamma_r^{-1} \tilde{K}_r^\top) + \text{trace}(|\Lambda| \tilde{\Theta}^\top \Gamma_\Theta^{-1} \tilde{\Theta})\end{aligned}$$

In view of (11), the time derivative of V along the solution of the system is derived as

$$\begin{aligned}\dot{V} &= -\mathbf{e}_m^\top Q \mathbf{e}_m + 2 \text{trace}(|\Lambda| \tilde{\Theta}^\top \Gamma_\Theta^{-1} \dot{\tilde{\Theta}}) \\ &\quad + 2 \mathbf{e}_m^\top P [-B \Lambda \tilde{K}_x \mathbf{x} - B \Lambda \tilde{K}_r \mathbf{r} + B \Lambda \tilde{\Theta}^\top \Phi - B \Lambda \mathbf{d}] \\ &\quad + 2 \text{trace}(|\Lambda| \tilde{K}_x \Gamma_x^{-1} \dot{\tilde{K}}_x^\top) + 2 \text{trace}(|\Lambda| \tilde{K}_r \Gamma_r^{-1} \dot{\tilde{K}}_r^\top)\end{aligned}$$

where $Q \in \mathbb{R}^{n \times n}$ is defined in (10). Utilizing the property $\text{trace}(\mathbf{CD}^\top) = \mathbf{D}^\top \mathbf{C}$ and $\Lambda = \text{sign}(\Lambda)|\Lambda|$, where $\mathbf{C} \in \mathbb{R}^n$, $\mathbf{D} \in \mathbb{R}^n$ and $\text{sign}(\Lambda) = \text{diag}(\text{sign}(\lambda_1), \text{sign}(\lambda_2), \dots, \text{sign}(\lambda_m))$, we have

$$\begin{aligned}\dot{V} &= -\mathbf{e}_m^\top Q \mathbf{e}_m - 2 \mathbf{e}_m^\top P B \Lambda \mathbf{d} \\ &\quad + 2 \text{trace}\left(|\Lambda| \tilde{K}_x [-\mathbf{x} \mathbf{e}_m^\top P B \text{sign}(\Lambda) + \Gamma_x^{-1} \dot{\tilde{K}}_x^\top]\right) \\ &\quad + 2 \text{trace}\left(|\Lambda| \tilde{K}_r [-\mathbf{r} \mathbf{e}_m^\top P B \text{sign}(\Lambda) + \Gamma_r^{-1} \dot{\tilde{K}}_r^\top]\right) \\ &\quad + 2 \text{trace}\left(|\Lambda| \tilde{\Theta}^\top [\Phi \mathbf{e}_m^\top P B \text{sign}(\Lambda) + \Gamma_\Theta^{-1} \dot{\tilde{\Theta}}]\right)\end{aligned}$$

By virtue of the adaptive laws (8)-(9), it follows that $\mathbf{e}_m(t)$, $\tilde{K}_x(t)$, $\tilde{K}_r(t)$, and $\tilde{\Theta}(t)$ are bounded since

$$\dot{V} = -\mathbf{e}_m^\top Q \mathbf{e}_m - 2 \mathbf{e}_m^\top P B \Lambda \mathbf{d} \quad (21)$$

Thanks to Young's inequality, it's easy to obtain that

$$-2 \mathbf{e}_m^\top P B \Lambda \mathbf{d} \leq \|\mathbf{e}_m\|^2 + \lambda_{\max}^2(P) \|B \Lambda \mathbf{d}\|^2$$

Therefore, (21) can be further rewritten as

$$\dot{V} \leq -(\lambda_{\min}(Q) - 1) \|\mathbf{e}_m\|^2 + \lambda_{\max}^2(P) \|B \Lambda \mathbf{d}\|^2 \quad (22)$$

In terms of the usual argument with Barbalat's lemma, the boundedness of $\mathbf{e}_m(t)$ can be guaranteed for $t \in [0, T_f]$ and

$$\lim_{t \rightarrow \infty} \mathbf{e}_m(t) = \frac{\lambda_{\max}(P)}{(\lambda_{\min}(Q) - 1)^{\frac{1}{2}}} \|B \Lambda \mathbf{d}\| \triangleq \gamma_1(\mathbf{d}) \quad (23)$$

where $\gamma_1(\mathbf{d})$ is a class- \mathcal{K} function.

(T3): For clarity, here we emphasize the iteration number k as the argument. According to the definition of $\mathbf{e}(k, t)$, $\mathbf{e}_d(k, t)$ and $\mathbf{e}_m(k, t)$, it's easy to verify that $\mathbf{e}(k, t) = \mathbf{e}_d(k, t) + \mathbf{e}_m(k, t)$. Together with the results achieved in (T1) and (T2), we have

$$\lim_{k \rightarrow \infty} \|\mathbf{e}(k, t)\| \leq \lim_{k \rightarrow \infty} \|\mathbf{e}_d(k, t)\| + \lim_{k \rightarrow \infty} \|\mathbf{e}_m(t)\|$$

which is bounded for all $t \in [0, T_f]$. Moreover, due to the fact that $\lim_{k \rightarrow \infty} \|\mathbf{e}_{d,i}(k, t)\| = 0$, for all $i \in \mathcal{I}_n^{\rho^*}$, we have

$$\lim_{t \rightarrow \infty} \lim_{k \rightarrow \infty} \|\mathbf{e}_i(k, t)\| \leq \lim_{t \rightarrow \infty} \|(\mathbf{e}_m(t))_i\|$$

$$= \frac{\lambda_{\max}(P)}{(\lambda_{\min}(Q) - 1)^{\frac{1}{2}}} \|(B \Lambda \mathbf{d})_i\| \triangleq \gamma_2(\mathbf{d})$$

with a class- \mathcal{K} function $\gamma_2(\mathbf{d})$, and $(\cdot)_i$ represents the i -th elements of the vector.

(T4): Considering that $\mathbf{x}_d(t)$ is a given differentiable and bounded trajectory, together with the results obtained in (T1) and (T2), for all $t \in [0, T_f]$ and for all $k \geq 1$, we can conclude the boundedness of $\mathbf{x}_m(k, t)$, $\mathbf{x}(t)$ and $\mathbf{r}(k, t)$ from the definition of $\mathbf{e}_d(t)$, $\mathbf{e}_m(t)$ and (6), respectively. \square

Remark 2: Since the input matrix B is non-square, only a subset of states is able to asymptotically converge to the desired trajectory. Nevertheless, these states are typically the ones of interest in practical applications. This is essentially a limitation of the ILC technique. \triangleleft

Remark 3: Although each iteration has a finite running time T_f , in repetitive systems, the running time tends to infinity as the iteration number increases. This ensures time domain convergence of the controlled system. \triangleleft

IV. NUMERICAL EXAMPLES

This section applies the IL-MRAC scheme introduced in Section III to a double linkage pendulum system depicted in Fig. 2. We first illustrate the superiority of the proposed method over the conventional ILC and MRAC methods in certain tracking tasks. Then, the computation efficiency in terms of the low-cost ILC pre-train is demonstrated through a linear superposition example.

The double pendulum's dynamics [19] are given by (24), where m_1, m_2 are the masses of the linkages, L_1, L_2 are the lengths, c_1, c_2 are unknown friction coefficients at the joints, g is the gravitational acceleration, $x_1(t) = [\theta_1(t), \dot{\theta}_1(t)]^\top$, $x_2(t) = [\theta_2(t), \dot{\theta}_2(t)]^\top$ are the angular positions and velocity of the double pendulum, and $u(t) = [u_1(t), u_2(t)]^\top$ are the control variables denoting the motor torques at the joints. All units of physical quantities conform to the fundamental units of the International System of Units (SI).

The double pendulum system (24) is essentially nonlinear and features model uncertainty and external disturbance as well as unknown initial states. But, defining the $x(t) = [x_1(t)^\top, x_2(t)^\top]^\top$, it can be easily recast into the form of the dynamic system (1).

A. Velocity tracking example

In this example, the control goal is selected as driving the state $x_2(t)$ to track a step-like trajectory $y(t) = G_f(s)R_d(t) \in \mathbb{R}^2$ with filter $G_f(s) = \frac{20}{s^2 + 9s + 20}$ and

$$R_d(t) = \begin{cases} [0.05, 0.025]^\top, & t < 5 \\ [0.025, 0]^\top, & 5 \leq t < 10 \\ [0.1, 0.075]^\top, & t \geq 10 \end{cases}$$

The runtime duration for each iteration k is 20 seconds.

Here, the parameters of (24) are set to be $m_1 = m_2 = 0.1775$, $L_1 = L_2 = 2$, $c_1 = c_2 = 0.2$, $g = 9.8$. Initial states of (24) are set as $x(0) = [-0.05, 0, 0.05, 0]^\top$.

The reference model is specified as

$$A_m = \begin{bmatrix} 0 & 0 & 1 & 0 \\ 0 & 0 & 0 & 1 \\ -4 & 0 & -2 & 0 \\ 0 & -4 & 0 & -2 \end{bmatrix}, B_m = \begin{bmatrix} 0 & 0 \\ 0 & 0 \\ 1 & 0 \\ 0 & 1 \end{bmatrix}, x_m(0) = \begin{bmatrix} 0 \\ 0 \\ 0 \\ 0 \end{bmatrix},$$

and it is trivial to obtain the expression of desired trajectory $x_d(t) = [\frac{1}{s}y(t)^\top, y(t)^\top]^\top$.

The tuning parameters of control scheme are taken as $K = \text{diag}\{1, 1, 1, 1\}$, $Q = \text{diag}\{10, 10, 10, 10\}$, $\Gamma_x = \text{diag}\{200, 200, 200, 200\}$, $\Gamma_r = \text{diag}\{50, 50\}$, $\Gamma_\Theta = \text{diag}\{10, 10, 10, 10\}$, $\text{sign}(\Lambda) = \text{diag}\{1, 1\}$, and the initial values of each entry of $K_x(t)$, $K_r(t)$ and $\Theta(t)$ are set to be zero. The signal regressor $\Phi(\mathbf{x})$ is specified as follows:

$$\Phi(\mathbf{x}) = - \begin{bmatrix} \dot{\theta}_1 \\ \dot{\theta}_2 \\ \dot{\theta}_1 \cos(\theta_2 - \theta_1) \\ \dot{\theta}_2 \cos(\theta_2 - \theta_1) \end{bmatrix} \cdot \frac{360000}{5041(9 \cos^2(\theta_1 - \theta_2) - 16)}$$

The iteration history of the root mean square (RMS) velocity tracking error $\mathbf{e}_d(t)$ over a time period of 20s is shown in Fig. 4. It is evident that the states of the nominal model converge monotonically to the desired trajectories as the iteration number increases. Hence, one can imagine that, if the real plant features exactly the same system model and initial conditions as the nominal one, then the behavior of a conventional ILC will be as good as the proposed controller. However, once such consistency is absent, the conventional ILC becomes no longer implementable in this example. In contrast, the success tracking achieved by our controller is clearly depicted in Fig. 5. Furthermore, we compare the performance between the proposed method and a classical MRAC method there. Indeed, both methods can guarantee the boundedness of trajectories and zero-convergence of the steady-state tracking errors. But it is worth drawing the reader's attention to the green box in Fig. 5 which shows that the proposed algorithm is capable of directly tracking the desired trajectories.

B. Superiority validation example

Another important merit of the proposed controller is the computational efficiency, in the sense that, in the proposed framework, the ILC-loop learning can be completely done offline, as the subject to be trained is merely a numerical nominal model. This property allows us to pre-train and store a large amount of good reference signals $\mathbf{r}(t)$ for different trajectories $\mathbf{x}_d(t)$. Nevertheless, if the desired trajectory encountered by the real application is still a brand-new one, the proposed IL-MRAC is capable of finding a suitable reference signal by directly combining the existing ones because the system we considered essentially satisfies the superposition principle. We will show how this can be done next.

Assume we have obtained three 'ideal' reference signals $\mathbf{r}_1(t), \mathbf{r}_2(t), \mathbf{r}_3(t)$ for three different desired trajectories $x_{d,1}(t) = 0.3 \sin(0.8t)$, $x_{d,2}(t) = 0.3 \sin(1.2t)$, $x_{d,3}(t) = 0.5 \sin(4t)$, respectively. Now, the plant (24) needs to track a new trajectory specified as follows

$$x_d(t) = 0.1x_{d,1}(t) + 0.2x_{d,2}(t) + 0.3x_{d,3}(t)$$

We use two strategies to approach this challenge: 1) direct training of the model in ILC-loop to track the desired trajectory directly and gain a new reference signal $\mathbf{r}(t)$; 2) without any training, we calculate the reference signal

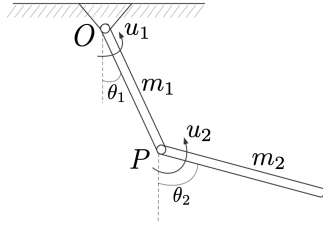


Fig. 2. Schematic of the double pendulum.

$$\begin{aligned}
 & \frac{1}{3} (m_1 + 3m_2) L_1^2 \ddot{\theta}_1 + \frac{1}{2} m_2 L_1 L_2 \ddot{\theta}_2 \cos(\theta_2 - \theta_1) - \frac{1}{2} m_2 L_1 L_2 \dot{\theta}_2^2 \sin(\theta_2 - \theta_1) \\
 & + \frac{1}{2} (m_1 + 2m_2) g L_1 \sin \theta_1 + (c_1 + c_2) \dot{\theta}_1 - c_2 \dot{\theta}_2 = u_1 + u_2 \\
 & \frac{1}{3} m_2 L_2^2 \ddot{\theta}_2 + \frac{1}{2} m_2 L_1 L_2 \ddot{\theta}_1 \cos(\theta_2 - \theta_1) + \frac{1}{2} m_2 L_1 L_2 \dot{\theta}_1^2 \sin(\theta_2 - \theta_1) \\
 & + \frac{1}{2} m_2 g L_2 \sin \theta_2 + c_2 \dot{\theta}_2 = u_2
 \end{aligned} \tag{24}$$

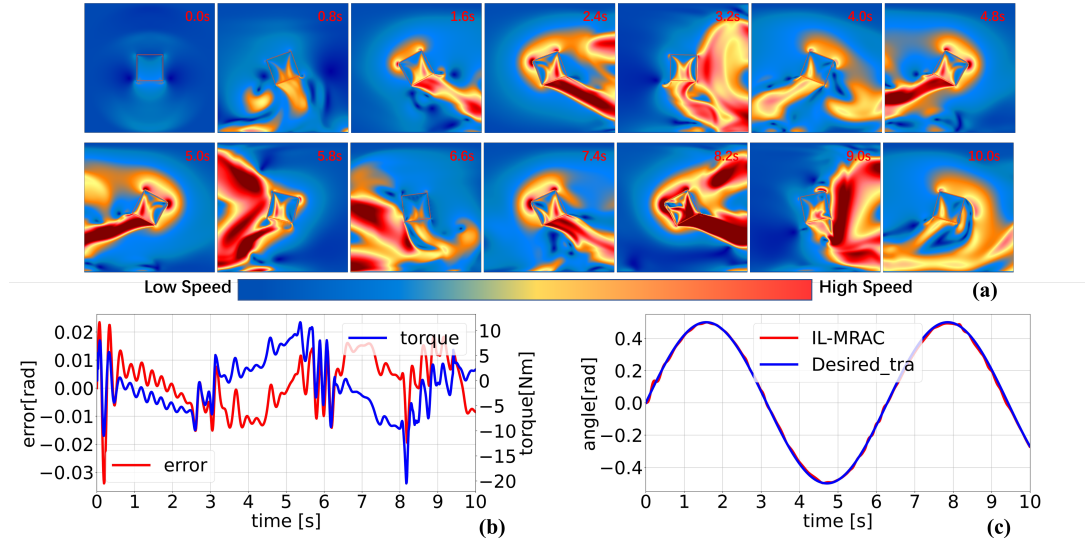


Fig. 3. **Simulation results.** A sin-type trajectory tracking in high-fidelity Simulator. The red region of (a) denotes high-speed airflow, while the blue region denotes low-speed airflow; the red line of (b) represents tracking error, while the blue line represents the generated torque by the controller; (c) is the final tracking performance.

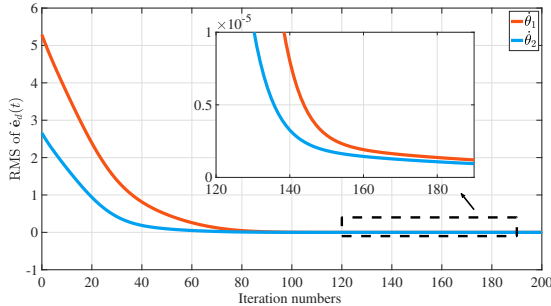


Fig. 4. Iterative evolution of the velocity tracking error $e_d(t)$.

$$\mathbf{r}'(t) = 0.1\mathbf{r}_1(t) + 0.2\mathbf{r}_2(t) + 0.3\mathbf{r}_3(t).$$

Next, substitute $\mathbf{r}(t)$ and $\mathbf{r}'(t)$ into the MRAC-loop. As depicted in Fig. 6, the complete overlapping of two trajectories indicates that, even the system to be controlled is nonlinear, we can dramatically save the time and computation cost in ILC-loop training by utilizing the existing data.

V. HIGH-FIDELITY SIMULATOR STUDY

In this section, a high-fidelity fluid simulation platform based on a recently proposed GPU-optimized lattice Boltzmann solver [24], [25] is used to simulate an attitude tracking problem of a 2D jet-controlled robot operating in a non-quiescent fluid field. This high-fidelity simulation platform is capable of generating vortex and turbulence flows that closely resemble the phenomena in the real-world. Therefore,

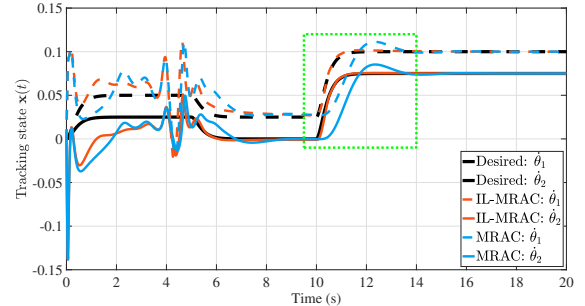


Fig. 5. Time evolution of state $x(t)$.

it can be used to validate the feasibility of the proposed scheme in practical applications.

The air density in the simulator is set to 1.225 kg/m^3 , and the viscosity is $1.81 \times 10^{-5} \text{ kg/(ms)}$, consistent with standard atmospheric pressure. The simulator's space size is $2\text{m} \times 1\text{m}$, and the grid resolution is 500×250 . Each grid corresponds to $4\text{mm} \times 4\text{mm}$ in reality. The controlled object's weight and length are 1 kg and 0.2 m, respectively. Additionally, the controlled object is placed inside a pipe, and a uniform flow of 0.4 m/s from top to bottom is considered to simulate the airflow experienced during flight. As the current solver has high requirements for both CPU and GPU performance, we conducted all experiments using an Intel Xeon Gold 6226R and Nvidia RTX 3090. The square

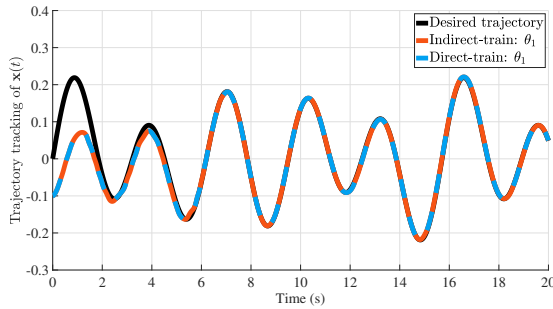


Fig. 6. Training results of IL-MRAC scheme under different methods.

appearance was chosen instead of a streamlined form to amplify the effect of turbulence flow and make the control task more challenging. The results of the 2D jet-controlled robot are shown in Fig. 3. Fig. 3 (a) presents a series of snapshots depicting sin-type trajectory tracking results. It can be seen that the vortices at the nozzle and top of the square object are strong and complex. This presents a significant challenge for the IL-MRAC controller to track the desired trajectories. However, as shown in Fig. 3 (b) and (c), the error and the output of the controller possess a reasonably similar behavior, and the tracking error remains within a small bound, which indicates the proposed scheme demonstrates a strong ability to cope with a nonlinear and complex task. The video of experimental results can be viewed at <https://www.youtube.com/watch?v=8e2DULTvmFU>.

VI. CONCLUSION

An indirect ILC-embedded MRAC scheme has been developed for a certain class of nonlinear uncertain MIMO systems under the effect of external disturbances and unknown initial states. By decoupling the ILC-loop and MRAC-loop in the iterative and time directions, the proposed method distinguishes itself from existing indirect-type ILC algorithms. In addition, via reusing the nominal model and reference signal, the presented framework circumvents their limitations (i.e. assumption and reference model design) while preserving their advantages (direct tracking and good adaptation ability). The effectiveness and superiority of the proposed algorithm have been demonstrated through numerical examples and high-fidelity experiments. It should be noted that the ILC and MRAC techniques utilized in the framework can be substituted with more advanced versions from related fields, provided that stability conditions listed in our paper are satisfied. For the purposes of elucidating the core concepts of the framework, two classic ILC and MRAC techniques are selected. This novel framework has the potential to broaden the application range of ILC and MRAC.

REFERENCES

- [1] G. Sebastian, Z. Li, Y. Tan, and D. Oetomo, “Analysis and experimental verification of a current-cycle iterative learning control for robotic manipulators with output constraints,” in *Proc. 58th IEEE Conf. Decis. Control (CDC)*, 2019, pp. 7468–7473.
- [2] A. Buelta, A. Olivares, E. Staffetti, W. Aftab, and L. Mihaylova, “A gaussian process iterative learning control for aircraft trajectory tracking,” *IEEE Trans. Aerosp. Electron. Syst.*, vol. 57, no. 6, pp. 3962–3973, 2021.
- [3] D. Huang, W. Yang, T. Huang, N. Qin, Y. Chen, and Y. Tan, “Iterative learning operation control of high-speed trains with adhesion dynamics,” *IEEE Trans. Control Syst. Technol.*, vol. 29, no. 6, pp. 2598–2608, 2021.
- [4] M. Yu and C. Li, “Robust adaptive iterative learning control for discrete-time nonlinear systems with time-iteration-varying parameters,” *IEEE Trans. Syst., Man, Cybern. Syst.*, vol. 47, no. 7, pp. 1737–1745, 2017.
- [5] D. Meng and K. L. Moore, “Contraction mapping-based robust convergence of iterative learning control with uncertain, locally lipschitz nonlinearity,” *IEEE Trans. Syst., Man, Cybern. Syst.*, vol. 50, no. 2, pp. 442–454, 2020.
- [6] G. Tao, “Multivariable adaptive control: A survey,” *Automatica*, vol. 50, no. 11, pp. 2737–2764, 2014.
- [7] R. Franco, H. Rios, A. F. de Loza, and D. Efimov, “A robust nonlinear model reference adaptive control for disturbed linear systems: An lmi approach,” *IEEE Trans. Autom. Control*, vol. 67, no. 4, pp. 1937–1943, 2022.
- [8] K. Barton and D. Kingston, “Systematic surveillance for uavs: A feed-forward iterative learning control approach,” in *Proc. Amer. Control Conf. (ACC)*, 2013, pp. 5917–5922.
- [9] Y. Hui, R. Chi, B. Huang, and Z. Hou, “Extended state observer-based data-driven iterative learning control for permanent magnet linear motor with initial shifts and disturbances,” *IEEE Trans. Syst., Man, Cybern. Syst.*, vol. 51, no. 3, pp. 1881–1891, 2021.
- [10] P. Pakshin, J. Emelianova, E. Rogers, and K. Galkowski, “Iterative learning control of stochastic linear systems with reference trajectory switching,” in *Proc. 60th IEEE Conf. Decis. Control (CDC)*, 2021, pp. 6572–6577.
- [11] G. Zhang, J. Wang, P. Yang, and S. Guo, “A learning control scheme for upper-limb exoskeleton via adaptive sliding mode technique,” *Mechatronics*, vol. 86, p. 102832, 2022.
- [12] D. Meng and K. L. Moore, “Robust iterative learning control for nonrepetitive uncertain systems,” *IEEE Trans. Autom. Control*, vol. 62, no. 2, pp. 907–913, 2017.
- [13] R. Chi, Z. Hou, and J. Xu, “Adaptive ilc for a class of discrete-time systems with iteration-varying trajectory and random initial condition,” *Automatica*, vol. 44, no. 8, pp. 2207–2213, 2008.
- [14] M. Yu and S. Chai, “Adaptive iterative learning control for discrete-time nonlinear systems with multiple iteration-varying high-order internal models,” *Int. J. Robust Nonlinear Control*, vol. 31, no. 15, pp. 7390–7408, 2021.
- [15] M. Sun and D. Wang, “Iterative learning control with initial rectifying action,” *Automatica*, vol. 38, no. 7, pp. 1177–1182, 2002.
- [16] J. Zhang and D. Meng, “Iterative rectifying methods for nonrepetitive continuous-time learning control systems,” *IEEE Trans. Cybern.*, vol. 53, no. 1, pp. 338–351, 2023.
- [17] G. Song and G. Tao, “A partial-state feedback model reference adaptive control scheme,” *IEEE Trans. Autom. Control*, vol. 65, no. 1, pp. 44–57, 2020.
- [18] R. B. Anderson, J. A. Marshall, and A. L’Afflitto, “Constrained robust model reference adaptive control of a tilt-rotor quadcopter pulling an unmodeled cart,” *IEEE Trans. Aerosp. Electron. Syst.*, vol. 57, no. 1, pp. 39–54, 2021.
- [19] N. T. Nguyen, *Model-Reference Adaptive Control*. Cham: Springer International Publishing, 2018, pp. 83–123.
- [20] C.-J. Chien and C.-Y. Yao, “An output-based adaptive iterative learning controller for high relative degree uncertain linear systems,” *Automatica*, vol. 40, no. 1, pp. 145–153, 2004.
- [21] ———, “Iterative learning of model reference adaptive controller for uncertain nonlinear systems with only output measurement,” *Automatica*, vol. 40, no. 5, pp. 855–864, 2004.
- [22] S. Jingzhuo and W. Huang, “Model reference adaptive iterative learning speed control for ultrasonic motor,” *IEEE Access*, vol. 8, pp. 181 815–181 824, 2020.
- [23] G. Tao, *Adaptive Control Design and Analysis*. Wiley, 2003.
- [24] W. Li, Y. Chen, M. Desbrun, C. Zheng, and X. Liu, “Fast and scalable turbulent flow simulation with two-way coupling,” *ACM Trans. Graph.*, vol. 39, no. 4, 2020.
- [25] W. Liu, K. Bai, X. He, S. Song, C. Zheng, and X. Liu, “Fishgym: A high-performance physics-based simulation framework for underwater

robot learning,” in *IEEE Int. Conf. Robot. Autom. (ICRA)*, 2022, pp. 6268–6275.